Interaction between Fine Particles of Fluorapatite and Phosphoric Acid Unraveled by Surface Spectroscopies

O.B. Kaba, L.O. Filippov, I.V. Filippova, M. Badawi

Version of Record: https://www.sciencedirect.com/science/article/pii/S0032591020312250
Manuscript_b4b944ab7bb6191d963c6803b0c815fb

Interaction between fine particles of fluorapatite and phosphoric acid unraveled by surface spectroscopies ~~to flotation~~

O. B. Kaba[1,3], L. O. Filippov[1*], I. V. Filippova[1], M. Badawi[2]

[1]*Université de Lorraine, CNRS, Georessources, 54500 Nancy, France.*

[2]*Université de Lorraine, CNRS, Laboratoire de Physique et Chimie Théoriques, 54500 Nancy, France.*

[3]*Institut Supérieur des Mines et Géologie de Boké (ISMGB), BP. 84, Boké, Guinea.*

*corresponding authors email : lev.filippov@univ-lorraine.fr

Abstract

Flotation mechanisms of calcareous phosphates ores, and in particular the reaction between phosphoric acid and fluorapatite have still to be elucidated. In the present work, variations of carbonated hydroxyfluorapatite (C-HFAp) in contact with various concentrations of phosphoric acid were studied using *ex-situ* and *in-situ* techniques, namely Raman and Infrared spectroscopy, X-Ray diffraction (XRD) and Scanning Electron microscopy (SEM). Raman spectra showed a calcium carbonate peak ($CaCO_3$) (1085 cm^{-1}) at low acid concentrations (between 10^{-3} and 10^{-2} $mol.L^{-1}$), disappearing at higher concentrations. Similarly, kinetic studies showed that, even if $CaCO_3$ appeared after 2 min reaction, it disappeared after 3 min. IR spectra and diffractograms seemed to display the presence of $CaCO_3$ at low acid concentrations (peak at 713 cm^{-1} on the IR spectra), with a change in $CaCO_3$ crystallinity and in the C-HFAp surface with increasing acid concentrations (broadening of the peak). Our results highlight the conversion of hydroxyfluoroapatite at high acid concentrations, with a coating of the mineral surface which prevents the dissolution of the mineral and can impact the adsorption of collectors. Our work contributes to the understanding of the mechanisms of depression of apatite minerals in phosphate ores flotation.

Keywords: Carbonated hydroxyfluorapatite; phosphoric acid; flotation; Raman and infrared spectroscopies.

1. Introduction

Phosphates are a fundamental finite resource, mainly used (> 90%) in agriculture for fertilizers production. Agriculture depends on phosphate ores because they are nonrecyclable, and currently, no minerals can replace them. Moreover, the increasing world crop production results in an increasing phosphate demand (Sis and Chander, 2003). Among the main phosphate ores (sedimentary, igneous or biogenic), sedimentary phosphates with a siliceous gangue are readily processable for fertilizers production. However, the rarefaction of siliceous phosphate resources results in the exploitation of phosphate ores with a carbonate gangue, which are considerably more complex and difficult to process than siliceous phosphates (Al-Fariss et al., 2014). Numerous laboratory and pilot plant studies were performed for extracting apatite (main phosphate bearing mineral), which represents more than 80% of the globe's phosphate reserve (Sis and Chander, 2003). Actually, flotation is the major process used for apatite extraction, allowing more than 60% of the worldwide phosphate recovery (Sis and Chander, 2003). The process performances are influenced by several variables such as the ore composition, particle size, reagents type, and ionic species present in the mineral pulp (Santana et al., 2008).

Apatites (hydroxylapatite, fluorapatite, francolite, etc) are the predominant phosphate minerals of sedimentary phosphates ores, while gangue commonly comprises silicates, metal oxides, carbonates and fluorite (Ashraf et al., 2005). Among these minerals, apatite, calcite, dolomite, barite, fluorite, scheelite, and any salt-type minerals which are highly soluble in aqueous media may be easily separated by flotation from oxides and silicates (Filippov et al., 2012). However, the separation of these minerals from each other is complex because of the presence of similar alkaline earth cations in their structure, leading to identical surface properties, and therefore close reactivity towards flotation collectors and depressants (El-Midany 2004, Filippova et al., 2014). Additionally, their close zero point of charge (ZPC), ranging between pH 4.5–5 results in similar electrokinetic properties of phosphates and carbonates, adding difficulty to their separation (El-Midany, 2004, Filippov et al., 2012). However, pH is a key parameter for the stability of calcium phosphates (Elliott, 1994) and for carbonate flotation (Gharabaghi et al. 2007). Moreover, complex reactions occur between dissolved species and mineral surfaces during flotation, modifying surficial properties and in consequence, separation performances (Yuehua et al. 1994). Therefore, the separation of these minerals requires additional treatments.

Calcite-dolomite-type impurities and phosphates show a similar response towards anionic and cationic collectors, resulting in separation difficulties (Abouzeid et al., 2009; Elgillani and Abouzeid, 1993; Gharabaghi et al., 2007; Mishra, 1978; Somasundaran et al., 1985).

Concerning the separation of apatite/calcite, which is the subject of the present work, one treatment consists in depressing apatite and preventing collectors adsorption on its surface. Among the various acidic depressants used (H_3PO_4, H_2SO_4, KH_2PO_4, $C_2H_2O_4$, H_2SiF_6, HF, tannic acid), phosphoric acid is the most commonly used, and the most efficient for separating phosphates from carbonates (calcite, dolomite) through reverse flotation (Abdel-Khalek, 2000; Zhang et al., 2007). This method leads to rather good separation results between apatite and carbonates, with the obtention of marketable phosphate concentrates as indicated as follows:

- 21.7% P_2O_5 grade and 65.5% recovery from a feed containing 5.0% P_2O_5, 45.8% CaO and 6.7% SiO_2 (Mohammadkhani et al., 2011);
- 15-30% P_2O_5 grade from an original mineral comprising 5.6% P_2O_5, 51.1% CaO and 7.4% SiO_2 (Hernáinz et al., 2004);
- 27.2% P_2O_5 grade with 73% recovery from ore containing 12.5% P_2O_5, 32% CaO and 26.5% SiO_2 (Prasad et al., 1995).

Mechanisms responsible for these good separation performances remain poorly understood. Several studies indicated a passivation of the apatite surface by a new layer formed (Abouzeid et al., 2009; Chaïrat et al., 2007; Dorozhkin, 2002; Schaad et al., 1997; Somasundaran et al., 1985), whose nature depends on the type and the strength of the acid used as depressant. Reactivity studies carried out on calcite-phosphoric acid and apatite-phosphoric acid systems showed the formation of a calcium-rich layer on the minerals. Performing chemical equilibria in heterogeneous systems with apatite and calcite, Somasundaran et al. (1985) mentioned a coverage of the apatite surface by monetite, at a pH below 4.8. Chaïrat et al. (2007) investigations on fluorapatite (FAP) dissolution in aqueous media showed the alteration of the fluorapatite surface, with a fast decrease of the Ca/F ratio and an enrichment in P, through chemical interactions between dissolved species at the FAP surface (H^+ and Ca^{2+}, OH^- and F^-). Chaïrat and co-workers (2007) indicated that the newly-formed layer was a dicalcium phosphate or monetite ($CaHPO_4$) leading to an apparent low solubility of FAP.

Most proposed mechanisms for controlling apatite reactivity in acidic media are based either on hypothesis or thermodynamics calculations. Although numerous experimental studies have been performed, using analytical techniques such as infrared spectroscopy (Fowler, 1974), XRD (Dickens et al., 1972), Raman spectroscopy (Klasa et al., 2013) and atomic force microscopy (Klasa et al., 2013), interactions between apatite and inorganic acids resulting in apatite depression have still to be elucidated.

The present work involved a range of analytical techniques for obtaining complementary results on the reactivity of carbonated hydroxyfluoroapatite (C-HFAp) with phosphoric acid, and more particularly to identify surface products which may affect flotation. Chemical species produced on the apatite surface have been monitored as a function of the concentration of phosphoric acid and the exposure time, using *in-situ* and *ex-situ* Raman and infrared spectroscopies, X-ray diffraction and scanning electron microscopy.

2. Materials and experimental procedure

2.1. Materials

The C-HFAp sample was obtained in Madagascar and the ICP-OES/MS (Table 1) and XRD (Fig. 1) analyses revealed the presence of small amounts of quartz and impurities such as caesium, thallium and lanthanum.

The Ca/P and Ca/F ratios of the sample (1.79 and 5.96, respectively), determined through chemical analyses (Table 1), differ from the theoretical stoichiometry of apatite (Ca/P = 1.67 and Ca/F = 5). They indicate a deficiency in both phosphate and fluorine relatively to calcium, which may be due to the substitution of phosphate and fluorine in the lattice, by carbonates as it is the case in carbonated apatite (Chhettry et al., 1999). This could be confirmed by the non-negligible loss on ignition (LOI) value that may indicate the presence of a small amounts of carbonate in the sample (<1%). Its BET surface area is 0.8 m^2/g.

Phosphoric acid of high-purity grade (Aldrich) was used in the experiments.

2.2. Analytical methods

The pH was measured with a pH meter (pH 3110, WTW) calibrated with pH 4.01, 7.00 and 10.0 standard solutions. pH-control was performed using a pH monitor (pH 170, WTW), with the addition of concentrated solutions of phosphoric acid.

The mineralogical composition of the samples was determined using XRD, with a Bruker D8 instrument using Co Kα radiation at a wavelength of 1.789 Å.

The chemical compositions of the minerals were determined using a Perkin Elmer Elan apparatus comprising an ICP-OES Icap 6500 with radial torch (Thermoscientific) for major component analysis, associated to an ICP-MS X7 (Thermoscientific) (without pre-concentration of REE and U/Th) for traces analysis.

An Ion 450 millivoltmeter (MeterLab) equipped with a specific electrode was used to analyse fluorine.

The particle morphology was observed using a HITACHI 500 SEM equipped with a Si-Li X-ray detector and a back scattered electron detector (KE Development).

Infrared spectra were measured using a Bruker IFS 55 spectrometer (with a GLOBAR SiC source and a MCT detector) equipped with a Harrick diffuse reflectance accessory.

Raman spectra were measured in the 200 - 4000 cm^{-1} wavenumber range using an RXN4 spectrometer (Kaiser) at a laser excitation wavelength of 532 nm, with a fiber-optic Raman sampling probe. The sapphire-head probe produces Raman peaks at 377, 417, 447, 576 and 749 cm^{-1}.

2.3. Experimental procedure

A 3 g sample of C-HFAp in the particle size range 20-100 µm was added to 100 ml of deionized water or phosphoric acid solutions at concentrations of 0.001, 0.01, 0.1, 0.25 and 0.5 M, and stirred at 200-300 rpm during 15 minutes. The pH of the solution and the Raman spectrum of the pulp were continuously recorded. After 15 minutes conditioning, the pulp was filtered, and then dried in a desiccator for 24 hours at room temperature. The dry sample was analysed by Raman and IR spectroscopies, XRD and SEM. The Raman spectrum of C-HFAp in solution was also measured as a function of time with continuous addition of phosphoric acid to maintain the pH approximately constant at 4.6 (±0.1) during 15 minutes. This continuous addition of concentrated H_3PO_4 injection only led to a slight variation in the solid/liquid ratio from 30 to ~29 g/l, but did not significantly affect the solubilisation rate.

The choice of phosphoric acid concentrations was (i) based on the conditioning pH used to separate phosphate ores from a carbonate gangue (calcite, dolomite) by flotation in acidic media; (ii) performed in order to investigate the reactivity of fluorapatite with phosphoric acid

under pH variations. According to the flowsheet (Abdel-Khalek et al., 2014; Mohammadkhani et al., 2011; Rao et al., 1985), the total conditioning time of the reagents (depressant, collector) during the separation of the phosphate ores from a carbonated gangue by flotation in acidic media varies between 5 and 11 minutes. In this study, 15 minutes reaction time for each test was chosen for analysing the reactivity between fluorapatite and phosphoric acid over a prolonged conditioning time.

3. Results and discussion

3.1. Raman spectroscopy

3.1.1. Raman spectroscopy of phosphoric acid

Raman spectra of phosphoric acid (without mineral) at various concentrations are shown in Fig. 2. These spectra show three peaks with intensities increasing with the concentration of phosphoric acid: a major one at 890 cm^{-1}, and two other peaks of lower intensity at 1075 cm^{-1} and 1174 cm^{-1}. These peaks, which appear from a concentration of 0.1 $mol.L^{-1}$ phosphoric acid, correspond to symmetric PO_4 vibrations (Brandão et al., 2009).

3.1.2. Raman spectroscopy of C-HFAp

Raman spectra of C-HFAp after 15 minutes contact with phosphoric acid at various concentrations are shown before (Figs. 3 and 4a) and after filtration and drying (Fig. 4b).

The spectrum of C-HFAp without phosphoric acid (Fig. 3, C = 0 $mol.L^{-1}$) presents a broad and intense peak around 3450 cm^{-1} due to OH vibrations (de Ligny et al., 2013), and a smaller peak at 963 cm^{-1} due to ν_1PO_4 vibrations (Casciani and Condrate, 1980). The shape, intensity and position of these two peaks remain constant with increasing the concentration of phosphoric acid.

From 0.25 $mol.L^{-1}$ phosphoric acid, a νPO_4 peak appears at 890 cm^{-1}, and its intensity increases with the concentration of phosphoric acid. This peak, also observed in Fig. 2, corresponds to phosphoric acid. Fig. 4 shows in details the spectral region 800-1200 cm^{-1}. In particular, in Fig. 4a (without filtration nor drying of C-HFAp) a new peak is present at 1085 cm^{-1} at 10^{-3} and 10^{-2} $mol.L^{-1}$ phosphoric acid. Another peak appears at 1078 cm^{-1} at 0.1 $mol.L^{-1}$ phosphoric acid which merges with the peak at 1085 cm^{-1} and makes it look broader. Although the intensity of the peak at 1078 cm^{-1} increases with the concentration of phosphoric acid, the intensity of the peak at 1085 cm^{-1} also increases up to 10^{-3} $mol.L^{-1}$

phosphoric acid but decreases above this concentration. Attribution of the peak present at 1085 cm^{-1} is complex, because it could be due either to PO_4 or CO_3 vibrations, according to Table 2 which shows the assignments of Raman bands from 1070 to 1088 cm^{-1} in relation with various minerals. Results of band component analysis of the Raman spectra are reported in Table 3. The peak at 1085 cm^{-1} has been assigned to ν_3PO_4 vibrations (Brandão et al., 2009; Casciani and Condrate, 1980), and also to ν_1CO_3 vibrations in other studies (Klasa et al., 2013; Termine and Lundy, 1974). Termine and Lundy (1974) investigated the PO_4 vibration of some phosphate salts and assigned the peaks at 1086-1088 cm^{-1} to νPO_4 in calcium phosphate and magnesium phosphate materials, but the authors found no νPO_4 peak in the 1086-1088 cm^{-1} region for calcium carbonate phosphates. They explained this absence with a dominant ν_1CO_3 band in this region for carbonate phosphates. In the present work, the Raman spectrum of untreated C-HFAp shows a peak at 1085 cm^{-1}. When the sample is brought in contact with phosphoric acid, the intensity of the peak at 1085 cm^{-1} increases up to 10^{-3}-10^{-2} $mol.L^{-1}$ phosphoric acid. It decreases, and the peak disappears at higher concentrations of phosphoric acid (Figs. 4a and 4b). As we observed a strong peak at 1085 cm^{-1} in our recent Raman study for a sample of pure calcite (Filippov et al., 2019), the 1085 cm^{-1} peak observed in Figs. 4a and 4b is therefore attributed to a CO_3 vibrations, in agreement with previous studies (Klasa et al., 2013; Termine and Lundy, 1974).

It is likely that the peak at 1078 cm^{-1}, or part of it, belongs to phosphoric acid (Fig. 2) as its intensity increases with phosphoric acid concentration, as for the peak at 890 cm^{-1}. Moreover, this peak is only observed at a phosphoric acid concentration of 0.1 $mol.L^{-1}$ and above, which is also the case for phosphoric acid (Fig. 2).

The Raman analysis performed on dried C-HFAp (Fig. 4b) confirms the previous spectral interpretations with, in particular, disappearance on the spectrum of both the 890 cm^{-1} and 1078 cm^{-1} peaks attributed to phosphoric acid which is removed by filtration, and presence of the peak at 963 cm^{-1} attributed to C-HFAp, the intensity of which remains constant (same amount of mineral in each experiment). Also, the behaviour of the peak at 1085 cm^{-1} is more clearly seen in Fig. 4b than in Fig. 4a because of the absence of the 1078 cm^{-1} adjoining peak; it is present in the absence of acid and increases in intensity up to a maximum value at 0.01 $mol.L^{-1}$ phosphoric acid before vanishing or drastically decreasing in intensity at higher acid concentrations (>0.1 mol L^{-1}). The major difference between Fig. 4a and Fig. 4b is the presence of a broad peak around 1052 cm^{-1} in the spectra of the dry sample. The intensity of this broad peak was lower for the sample in solution. It belongs to C-HFAp as it is also

present in the absence of phosphoric acid (Fig. 4a) and its intensity and shape remain constant. It is attributed to ν_3PO_4 vibrations (Nathanael et al., 2013; Penel et al., 1997).

The presence of calcium carbonate in the system for the pH ranging between 4.6 and 7.5 was attributed to a surface conversion phenomenon of apatite into calcite. Somasundaran and Wang (2006) indicated two possibilities that may occur if the apatite system is in contact with atmospheric CO_2 (as in this study): (i) calcite can precipitate with subsequently coating the apatite surface, (ii) the surface of apatite particles could be converted into calcite through various surface reactions leading to surface precipitation. In flotation, consequences of such phenomena are relevant, in particular for the separation of apatite from other calcium minerals (e.g. calcite, dolomite) by selective flotation. Thus, in the flotation of apatitic minerals, calcium carbonate newly formed by surface conversion of apatite probably acts as a coating layer on the apatite surface which prevents apatite dissolution on one hand and impact the adsorption of collectors on the other hand.

3.2. Infrared spectroscopy

Infrared spectra of C-HFAp as a function of phosphoric acid concentrations are shown in Figs. 5a, 5b and 5c for the spectral regions 4100-600 cm^{-1}, 900-670 cm^{-1} and 1600-1360 cm^{-1}, respectively. Table 3 shows the results of IR band component analysis together with the attribution of each band.

IR spectra are complex and present peaks attributed to OH vibrations at 3540 cm^{-1} (Arifuzzaman and Rohani, 2004), and to CO_3 and PO_4 vibrations. Contamination by silicates-probably quartz (Table 1 and Fig. 1) is shown by the presence of peaks at 804, 730, 695 and 1160 cm^{-1} attributed to ν(Si-O) (Hlavay et al., 1978). The presence of CO_3 peaks in the infrared spectra confirms that carbonate is present in the C-HFAp sample. The presence of CO_3 and OH in the sample may be the result of their substitutions with PO_4 and F respectively, in the crystal lattice of the untreated sample, as it is the case for carbonated hydroxy-fluorapatite (C-HFAp). Other authors report this similar type of apatite in their studies (Regnier et al., 1994).

Major changes observed with increasing phosphoric acid concentrations occur for some CO_3 peaks. In particular, new CO_3 peaks at 2987, 2879, 2514, 1795, 876, 848 and 713 cm^{-1}, which were absent in the spectrum of C-HFAp without phosphoric acid, appear in the spectra with 10^{-3} and 10^{-2} $mol.L^{-1}$ phosphoric acid, but their intensity decreases or peaks disappear at

higher acid concentrations (Fig. 5a). The peaks at 2987, 2879 and 2514 cm^{-1} are attributed to overtones of the stretching vibrations of ν_3CO_3 (Table 3) (Van Olphen and Fripiar, 1979). In the untreated sample, these peaks have a low intensity that becomes relatively intense in presence of phosphoric acid, particularly at 10^{-3} and 10^{-2} $mol.L^{-1}$. The peak at 1795 cm^{-1} (Fig. 5a) is due to an overtone of ν_3CO_3 vibration (Farmer, 1975). It is already present in the untreated sample and increases in intensity up to 10^{-2} $mol.L^{-1}$ phosphoric acid before decreasing at higher acid concentrations. The peaks at 876 and 848 cm^{-1} are also assigned to ν_2CO_3 (Regnier et al., 1994); they appear at 10^{-3} and 10^{-2} $mol.L^{-1}$ phosphoric acid (Fig. 5b). Regnier and co-workers indicated that these two peaks are characteristic of natural C-HFAp (Regnier et al., 1994). The ν_4 peak at 713 cm^{-1}, also appearing at 10^{-3} and 10^{-2} $mol.L^{-1}$, and disappearing when the phosphoric acid concentration reaches 10^{-1} $mol.L^{-1}$ (Fig. 5b), is attributed to CO_3 vibration (Farmer, 1975). However, Ren et al. (2014) attributed this peak to a CO_3 vibration of calcite, indicating the presence of detectable $CaCO_3$ formed on the C-HFAp surface during treatment at low phosphoric acid concentrations. The three peaks at 1454, 1425 (Fig. 5c) and 866 cm^{-1} (Fig. 5b) are due to ν_3CO_3 (Okazaki, 1983). These vibrations correspond to CO_3 ions which have substituted PO_4 ions in the C-HFAp lattice (Regnier et al., 1994). The weak or absence of phosphoric acid's influence on the intensity of the peaks at 1454, 1425 and 866 cm^{-1}, even at high acid concentrations, seems to be due to different structural states of CO_3 : ν_3CO_3-corresponding peak (1454, 1425 and 866 cm^{-1}) is probably for a better ordered state than the one corresponding to ν_4CO_3 (713 cm^{-1}). Thus, this difference in CO_3 structural state may lead to a differential dissolution, as it was reported that the substitution of PO_4 ions by CO_3 in the apatite lattice leads to structural disorder and also to higher solubility (Hontsu and Yoshikawa, 2015). A shoulder peak at 1544 cm^{-1} (Figs. 5a and 5c) due to ν_3CO_3 (Okazaki, 1983; Ren et al., 2014) appears at 10^{-1} $mol.L^{-1}$ phosphoric acid and is better defined at higher acid concentrations.

At least two types of carbonated apatite exist, called type A and type B (Ren et al., 2014). Type A can be prepared through hydrothermal route or by the reaction of apatite with CO_2 at a high temperature, while type B is prepared from aqueous precipitated carbonated apatite. Ren et al. (2014) found that type A has a characteristic CO_3 IR peak at 1546 cm^{-1} which corresponds to the CO_3 substitution for OH, while type B has a characteristic CO_3 IR peak at 1465 cm^{-1} which corresponds to the CO_3 substitution for PO_4 (Ren et al., 2014). They also reported that the IR peaks at 880, 1413 and 1450 cm^{-1} may also be attributed to type B, but

may also originate from carbonate adsorption on the apatite surface or to a separate intermixed carbonate containing phase (no substitution).

Peaks at 2143 – 1872 cm^{-1} due to overtones of ν_3PO_4 (Jouve, 1995) and peaks at 1086 – 933 cm^{-1} (Fig. 5a) assigned to ν_1PO_4 and ν_3PO_4 (Grunenwald et al., 2014) did not change significantly with variations in phosphoric acid concentration. However, the PO_4 large band at 1086 – 933 cm^{-1} seems to decrease in intensity and mostly becomes broader with increasing phosphoric acid concentration over 10^{-1} M. These changes in intensity and broadness indicate modifications in the C-HFAp structure/crystallinity after reaction with phosphoric acid. Drouet (2013) also observed a broadening of IR peaks as a function of crystallinity degrees, in infrared spectra of different Ca-phosphate.

3.3. XRD and SEM analysis of C-HFAp

Fig. 6 displays XRD patterns of C-HFAp. The sample has been 15 minutes in contact with phosphoric acid at concentrations ranging between 10^{-3} and 0.5 $mol.L^{-1}$, then filtrated and dried. All XRD patterns are compared to those in the database JCP2.ca. Fig. 6 shows no clear evidence for new crystalline phases in the XRD of C-HFAp after contact with phosphoric acid (Fig.6), except for a new peak at ~34° (d = 3.03) which only appears at phosphoric acid concentrations of 10^{-3} and 10^{-2} $mol.L^{-1}$. This peak is present in some Ca-phosphate compounds (e.g. brushite, pyrophosphate) but is also the main XRD peak of calcium carbonate (JCP2.ca 05-0586). As previously indicated, this peak corresponds to the main XRD peak of calcium carbonate. Calcium carbonate is indeed present in the C-HFAp sample (also identified in several other calcium phosphate materials, (Lu et al., 2000)) and clearly identified in the infrared spectra.

SEM images of C-HFAp samples are shown in Fig. 7. The surface and particle morphology appears unchanged after treatment with 0.5 $mol.L^{-1}$ phosphoric acid, indicating that no new mineral phases are produced at this high acid concentration. This observation is in contradiction with (Dorozhkin(1997) who observed the formation of a thin surface layer of acidic calcium phosphates ($CaHPO_4{\cdot}2H_2O$ and/or $Ca(H_2PO_4)_2{\cdot}H_2O$) on apatite treated with phosphoric acid.

3.4. Change of solution pH with phosphoric acid concentration

Variations of pH for C-HFAp pulp solution in contact with phosphoric acid are shown in Fig. 8a. From 0 to 10^{-2} mol.L^{-1} phosphoric acid, the pH increases rapidly in the first 2 minutes after addition of the mineral. It then remains constant, and slightly increases or decreases later up 15 minutes where it reaches an equilibrium. Moreover, pH values at equilibrium decrease with increasing the phosphoric acid concentration. They are higher than 6, for 0 to 10^{-2} mol.L^{-1} phosphoric acid, and become close to or lower than 2, at a phosphoric acid concentration of 10^{-1} mol.L^{-1} or higher. Phosphate minerals are known to be sparingly soluble (Valsami-Jones, 1998) and it was found that addition of C-HFAp to a phosphoric acid solution increases the pH, indicating a proton consumption by the C-HFAp surface and/or by C-HFAp dissolution products (Eq. 1).

$$PO_4^- + H^+ \Leftrightarrow \equiv PO_3H \quad Ca_5(PO_4)_3F + 3H^+ \Leftrightarrow 5Ca^{2+} + 3HPO_4^{2-} + F^- \qquad (1)$$

This proton consumption or pH-variation in solution (ΔpH in Fig. 8b) is drastically reduced at phosphoric acid concentrations above 10^{-2} mol.L^{-1}, which may be the result of surface passivation after formation of a new phase, at the surface or in solution, between dissolved calcium ions and phosphoric acid, followed by precipitation as suggested by Somasundaran et al (1985).

These pH-variations in solution following mineral addition are well known for semi-soluble minerals, and have been associated for calcite, to the hydrolysis of carbonate and calcium ions in solution after solubilisation of the mineral surface, with production of OH^- and H^+ respectively, according to Eqs. 2 and 3 (Somasundaran and Agar, 1967).

$$CaCO_3 \Leftrightarrow Ca^{2+} + CO_3^{2-} \qquad (2)$$

$$Ca^{2+} + H_2O \Leftrightarrow CaOH^+ + H^+ \text{ and } CO_3^{2-} + H_2O \Leftrightarrow HCO_3^- + OH^- \qquad (3)$$

The small pH-variation after 2 minutes contact of the solution with the mineral may be associated with the adsorption and/or precipitation of hydrolysis products (Eq. 3), resulting in the slow diffusion of protons at the mineral-solution interface (Somasundaran and Agar, 1967). Although different mechanisms at the solid-liquid interface may be involved to explain the fast and slow pH-variations observed in Fig. 8a (Somasundaran and Agar, 1967), these variations may be simply related to the relatively large range of particle sizes (20-100 µm) of samples used in the present, study with a quick dissolution of the finest particles, and a slower dissolution of the coarsest particles, as reported in the literature (Fulmer et al., 2002).

Variations in pH ($\Delta pH = pH_{t=15\ min} - pH_{t=0,\ without\ mineral}$) or proton consumption by the C-HFAp pulp (obtained from the results in Fig. 8a) is reported in Fig. 8b. The decrease in proton consumption at phosphoric acid concentration above 10^{-2} mol.L^{-1} seems to indicate a reduction of the C-HFAp dissolution at high concentrations of phosphoric acid. It may be the result of a mineral surface passivation after the formation of calcium phosphate species (e.g., monetite) on the surface or in solution, followed by their adsorption and/or precipitation (Somasundaran and Agar, 1967; Dorozhkin, 1996). Indeed, Somasundaran and co-workers (Somasundaran et al., 1985) have discussed the possibility a reduction of apatite solubility caused by a coating of calcium phosphate. Moreover, several studies have shown that the dissolution of apatite in phosphoric acid results in the formation of calcium phosphate species such as monetite or brushite (Larsen and Jensen, 1989), on the apatite surface (Valsami-Jones, 1998). Schaad et al. (1997) proposed a dissolution model where the proton diffusion process is restricted by spontaneous formation of an adsorbed calcium-rich layer at the solid interface.

5. Conclusion

The experimental approach used in the present work consisted in *in-situ* and *ex-situ* studies of the reactivity of C-HFAp in contact with various concentrations of phosphoric acid, by using Raman spectroscopy, infrared spectroscopy, XRD and SEM. Raman and infrared spectra as well as XRD patterns of C-HFAp showed the apparition and growth of new carbonate peaks attributed to calcium carbonate, between 10^{-3} and 10^{-2} mol.L^{-1} phosphoric acid concentration, and their decrease/disappearance at higher concentrations. Intensity- and shape-variations of infrared peaks indicated modifications of the C-HFAp structure/crystallinity with increasing phosphoric acid concentrations. The formation of this calcium carbonate phase on C-HFAp coincides with the decrease in mineral reactivity and more precisely proton consumption. Results obtained in this study may have a strong implication for the separation of apatite-from carbonate-minerals by flotation, and more particularly if this calcium carbonate phase reduces apatite dissolution and collector's adsorption processes.

Acknowledgements

The financial supports from Labex “Ressources21” (Strategic Metals in the 21st Century) contract ANR-10-LABX-0021 is gratefully acknowledged.

References

Abdel-Khalek, N.A., 2000. Evaluation of flotation strategies for sedimentary phosphates with siliceous and carbonates gangues. Minerals Engineering 13, 789–793.

Abdel-khalek, N.A., Selim, K.A., Abdallah, M.M., 2014. Flotation of Egyptian Newly Discovered Fine Phosphate Ore of Nile Valley, in: Proceedings of the International Conference on Mining, Material and Metallurgical Engineering. Prague, pp. 1–8.

Abouzeid, A.Z.M., Negm, A.T.T., Elgillani, D.A.A., 2009. Upgrading of calcareous phosphate ores by flotation: Effect of ore characteristics. International Journal of Mineral Processing 90, 81–89.

Al-Fariss, T.F., Arafat, Y., Abd El-Aleem, F.A., El-Midany, A.A., 2014. Investigating sodium sulphate as a phosphate depressant in acidic media. Separation and Purification Technology 124, 163–169.

Arifuzzaman, S.M., Rohani, S., 2004. Experimental study of brushite precipitation. Journal of Crystal Growth 267, 624–634.

Ashraf, M., Zafar, Z.I., Ansari, T.M., 2005. Selective leaching kinetics and upgrading of low-grade calcareous phosphate rock in succinic acid. Hydrometallurgy 80, 286–292.

Awonusi, A., Morris, M.D., Tecklenburg, M.M.J., 2007. Carbonate assignment and calibration in the Raman spectrum of apatite. Calcified tissue international 81, 46–52. https://doi.org/10.1007/s00223-007-9034-0.

Brandão, R.F., Quirino, R.L., Mello, V.M., Tavares, A.P., Peres, A.C., Guinhos, F., Rubim, J.C., Suarez, P.A.Z., 2009. Synthesis, characterization and use of Nb2O5 based catalysts in producing biofuels by transesterification, esterification and pyrolysis. Journal of the Brazilian Chemical Society 20, 954–966.

Casciani, F., Condrate, R.A., 1980. Raman spectrum of monetite, CaHPO4. Journal of Solid State Chemistry 34, 385–388.

Chaïrat, C., Oelkers, E.H., Schott, J., Lartigue, J.E., 2007. Fluorapatite surface composition in aqueous solution deduced from potentiometric, electrokinetic, and solubility measurements, and spectroscopic observations. Geochimica et Cosmochimica Acta 71, 5888–5900.

Chhettry, A., Wang, Z., Fox, J.L., Baig, A.A., Zhuang, H., Higuchi, W.I., 1999. Use of dicalcium phosphate dihydrate as a probe in an approach for accurate calculations of solution equilibria in buffered calcium phosphate systems. Journal of Colloid and Interface Science 218, 47–56. https://doi.org/10.1006/jcis.1999.6307.

de Ligny, D., Guillaud, E., Gailhanou, H., Blanc, P., 2013. Raman Spectroscopy of Adsorbed Water in Clays: First Attempt at Band Assignment. Procedia Earth and Planetary Science 7, 203–206.

Dickens, B., Bowen, J.S., Brown, W.E., 1972. A refinement of the crystal structure of CaHPO4 (synthetic monetite). Acta Crystallographica Section B Structural Crystallography and Crystal Chemistry 28, 797–806.

Dorozhkin, S. V., 2002. A review on the dissolution models of calcium apatites. Progress in Crystal Growth and Characterization of Materials 44, 45–61.

Dorozhkin, S. V., 1997. Acidic dissolution mechanism of natural fluorapatite. II. Nanolevel of investigations. Journal of Crystal Growth 182, 133–140. https://doi.org/10.1016/S0022-0248(97)00331-X.

Dorozhkin, S. V., 1996. Dissolution kinetics of single fluoroapatite crystals in phosphoric acid solution under the conditions of the wet-process phosphoric acid production. Journal für Praktische Chemie/Chemiker-Zeitung 338, 620–626. https://doi.org/10.1002/prac.199633801119.

Drouet, C., 2013. Apatite formation: why it may not work as planned, and how to conclusively identify apatite compounds. BioMed research international 2013, 12. https://doi.org/10.1155/2013/490946.

Elgillani, D.A., Abouzeid, A.Z.M., 1993. Flotation of carbonates from phosphate ores in acidic media. International Journal of Mineral Processing 38, 235–256.

El-Midany, A.A., 2004. Separating dolomite from phosphate rock by reactive flotation Fundamentals and application. Florida.

Farmer, V.C., 1975. Infrared spectroscopy in mineral chemistry, in: Physicochemical Methods of Mineral Analysis. Springer US, Boston, MA, pp. 357–388.

Filippov L., Duverger A., Filippova I., Kasaini H., Thiry J., 2012. - Selective flotation of silicates and Ca-bearing minerals: the role of non-ionic reagent on cationic flotation. Minerals Engineering, 36–38, (10) 314-323.

Filippova I.V., L.O. Filippov, A. Duverger, Severov. V.V., 2014. Synergetic effect of a mixture of anionic and nonionic reagents: Ca mineral contrast separation by flotation at neutral pH. Minerals Engineering, 66-68, 135-144.

Filippov, L.O., Kaba, O.B., Filippova, I.V., 2019. Surface analyses of calcite particles reactivity in the presence of phosphoric acid. Advanced Powder Technology. https://doi.org/doi.org/10.1016/j.apt.2019.06.026.

Fowler, B.O., 1974. Infrared studies of apatites. I. Vibrational assignments for calcium, strontium, and barium hydroxyapatites utilizing isotopic substitution. Inorganic Chemistry 13, 194–207.

Frost, R.L., Xi, Y., Scholz, R., López, A., Belotti, F.M., 2013. Vibrational spectroscopic characterization of the phosphate mineral hureaulite – (Mn, Fe)5(PO4)2(HPO4)2·4(H2O). Vibrational Spectroscopy 66, 69–75.

Fulmer, M.T., Ison, I.C., Hankermayer, C.R., Constantz, B.R., Ross, J., 2002. Measurements of the solubilities and dissolution rates of several hydroxyapatites. Biomaterials 23, 751–5.

Gadaleta, S.J., Paschalis, E.P., Betts, F., Mendelsohn, R., Boskey, A.L., 1996. Fourier transform infrared spectroscopy of the solution-mediated conversion of amorphous calcium phosphate to hydroxyapatite: New correlations between X-ray diffraction and infrared data. Calcified Tissue International 58, 9–16. https://doi.org/10.1007/s002239900004.

Gharabaghi, M., Noaparast, M., Shafaei Tonkaboni, S.Z., 2007. Lar mountain phosphate ore processing using flotation approach. Iranian Journal of Science and Technology. Transaction B, Engineering 31, 447–450.

Grunenwald, A., Keyser, C., Sautereau, A.M., Crubézy, E., Ludes, B., Drouet, C., 2014. Revisiting carbonate quantification in apatite (bio)minerals: A validated FTIR methodology. Journal of Archaeological Science 49, 134–141. https://doi.org/10.1016/j.jas.2014.05.004.

Hernáinz, F., Calero, M., Blázquez, G., 2004. Flotation of low-grade phosphate ore. Advanced Powder Technology 15, 421–433.

Hlavay, J., Jonas, K., Elek, S., Inczedy, J., 1978. Characterization of the particle size and the crystallinity of certain minerals by IR spectrophotometry and other instrumental methods: II, Investigations on quartz and feldspar. Clays and Clay Minerals 26, 139–143.

Hontsu, S., Yoshikawa, K., 2015. Ultra-thin hydroxyapatite sheets for dental applications, in: Publishing, W. (Ed.), Hydroxyapatite (Hap) for Biomedical Applications. pp. 129–142. https://doi.org/10.1016/B978-1-78242-033-0.00006-7.

Jouve, R.G., 1995. Caractérisation du tissu osseux par spectrométrie d'adsorption infrarouge. Université Jean Monnet Sainte-Etienne.

Juillard, A., Falgayrac, G., Cortet, B., Vieillard, M.H., Azaroual, N., Hornez, J.C., Penel, G., 2010. Molecular interactions between zoledronic acid and bone: An in vitro Raman microspectroscopic study. Bone 47, 895–904. https://doi.org/10.1016/j.bone.2010.07.018.

Klasa, J., Ruiz-Agudo, E., Wang, L.J., Putnis, C. V., Valsami-Jones, E., Menneken, M., Putnis, A., 2013. An atomic force microscopy study of the dissolution of calcite in the presence of phosphate ions. Geochimica et Cosmochimica Acta 117, 115–128.

Kodati, V.R., Tomasi, G.E., Turumin, J.L., Tu, A.T., 1991. Raman Spectroscopic Identification of Phosphate-Type Kidney Stones. Applied Spectroscopy 45, 581–583.

Lambert, J.B., Shurvell, H.F., Cook, G.B., 1987. Introduction to Organic Spectroscopy. Macmillan Publishing Company, New York.

Larsen, M.J., Jensen, S.J., 1989. Stability and mutual conversion of enamel apatite and brushite at 20 °C as a function of pH of the aqueous phase. Archives of Oral Biology 34, 963–968. https://doi.org/10.1016/0003-9969(89)90053-8.

Lu, H.B., Campbell, C.T., Graham, D.J., Ratner, B.D., 2000. Surface characterization of hydroxyapatite and related calcium phosphates by XPS and TOF-SIMS. Analytical Chemistry 72, 2886–2894. https://doi.org/10.1021/ac990812h.

Madejová, J., Komadel, P., 2001. Baseline studies of the clay minerals society source clays : infrared methods. Clays and Clay Minerals 49, 410–432. https://doi.org/10.1346/ccmn.2001.0490507.

Mandair, G.S., Morris, M.D., 2015. Contributions of Raman spectroscopy to the understanding of bone strength., BoneKEy reports. Nature Publishing Group. https://doi.org/10.1038/bonekey.2014.115.

Mishra, S.K., 1978. The electrokinetics of apatite and calcite in inorganic electrolyte environment. International Journal of Mineral Processing 5, 69–83.

Mohammadkhani, M., Noaparast, M., Shafaei, S.Z., Amini, A., Amini, E., Abdollahi, H., 2011. Double reverse flotation of a very low grade sedimentary phosphate rock, rich in carbonate and silicate. International Journal of Mineral Processing 100, 157–165.

Nathanael, J.A., Mangalaraj, D., Hong, S.I., Masuda, Y., Rhee, Y.H., Kim, H.W., 2013. Influence of fluorine substitution on the morphology and structure of hydroxyapatite nanocrystals prepared by hydrothermal method. Materials Chemistry and Physics 137, 967–976. https://doi.org/10.1016/j.matchemphys.2012.11.010.

Okazaki, M., 1983. F-CO3 Interaction in IR spectra of fluoridated CO_3-apatites. Calcified Tissue International 35, 78–81. https://doi.org/10.1007/BF02405010.

Penel, G., Cau, E., Delfosse, C., Rey, C., Hardouin, P., Jeanfils, J., Delecourt, C., Lemaître, J., Leroy, G., 2003. Raman microspectrometry studies of calcified tissues and related biomaterials. Dent. Med. Probl. 40, 37–43.

Penel, G., Leroy, G., Leroy, N., Behin, P., Langlois, J.M., Libersa, J.C., Dupas, P.H., 2000. Raman spectrometry applied to calcified tissue and calcium-phosphorus biomaterials. Bulletin du Groupèment international pour la recherche scientifique en stomatologie & odontologie 42, 55–63.

Penel, G., Leroy, G., Rey, C., Sombret, B., Huvenne, J.P., Bres, E., 1997. Infrared and Raman microspectrometry study of fluor-fluor-hydroxy and hydroxy-apatite powders. Journal

of Materials Science: Materials in Medicine 8, 271–276. https://doi.org/10.1023/A:1018504126866.

Potgieter-Vermaak, S.S., Potgieter, J.H., Van Grieken, R., 2006. The application of Raman spectrometry to investigate and characterize cement, Part I: A review. Cement and Concrete Research 36, 656–662.

Prasad, M., Majmudar, A.K., Rao, G.M., Rao, T.C., 1995. Flotation studies on a low-grade, cherty-calcareous rock phosphate ore from Jhabua, India. Minerals and Metallurgical Processing 12, 92–96.

Rao, D.V., Narayanan, M.K., Nayak, U.B., Ananthapadmanabhan, K., Somasundaran, P., 1985. Flotation of calcareous Mussorie phosphate ore. International Journal of Mineral Processing 14, 57–66.

Regnier, P., Lasaga, A.C., Berner, R.A., Han, O.H., Zilm, K.W., 1994. Mechanism of CO_3 substitution in carbonate-fluorapatite; evidence from FTIR spectroscopy, 13 C NMR, and quantum mechanical calculations. American Mineralogist 79, 809–818.

Ren, F., Ding, Y., Leng, Y., 2014. Infrared spectroscopic characterization of carbonated apatite: a combined experimental and computational study. Journal of biomedical materials research. Part A 102, 496–505. https://doi.org/10.1002/jbm.a.34720.

Sakae, T., 2006. Variations in dental enamel crystallites and micro-structure. Journal of Oral Biosciences 48, 85–93. https://doi.org/10.1016/S1349-0079(06)80021-6.

Santana, R.C., Farnese, A.C., Fortes, M.C., Ataíde, C.H., Barrozo, M.A., 2008. Influence of particle size and reagent dosage on the performance of apatite flotation. Separation and Purification Technology 64, 8–15.

Schaad, Ph., Poumier, F., Voegel, J.C., Gramain, Ph., 1997. Analysis of calcium hydroxyapatite dissolution in non-stoichiometric solutions. Colloids and Surfaces A: Physicochemical and Engineering Aspects 121, 217–228.

Sis, H., Chander, S., 2003. Reagents used in the flotation of phosphate ores: A critical review. Minerals Engineering 16, 577–585.

Somasundaran, P., Agar, G.E.E., 1967. The zero point of charge of calcite. Journal of Colloid and Interface Science 24, 433–440.

Somasundaran, P., Amankonah, J.O., Ananthapadmabhan, K.P., 1985. Mineral—solution equilibria in sparingly soluble mineral systems. Colloids and Surfaces 15, 309–333.

Somasundaran, P., Wang, D., 2006. Solution chemistry : minerals and reagents. Elsevier.

Termine, J.D., Lundy, D.R., 1974. Vibrational spectra of some phosphate salts amorphous to X-ray diffraction. Calcified Tissue Research 15, 55–70. https://doi.org/10.1007/BF02059043.

Valsami-Jones, E., 1998. The dissolution of apatite in the presence of aqueous metal cations at pH 2–7. Chemical Geology 151, 215–233. https://doi.org/10.1016/S0009-2541(98)00081-3.

Van Olphen, H., Fripiar, J.J., 1979. Data handbook for clay materials and other non-metallic minerals, Pergamon P. ed.

Xu, J., 1996. Vibrational Spectroscopic Investigations of Calcium Phophates and dental materials. McGil University, Montreal, Quebec, Canada.

Zhang, P., Snow, R., Peres, A.E.C., El-Shall, H., El-Midany, A., 2007. Depressants in non-sulfide mineral flotation. Froth Flotation: A Century of Innovation. Littleton: SME 555–574.

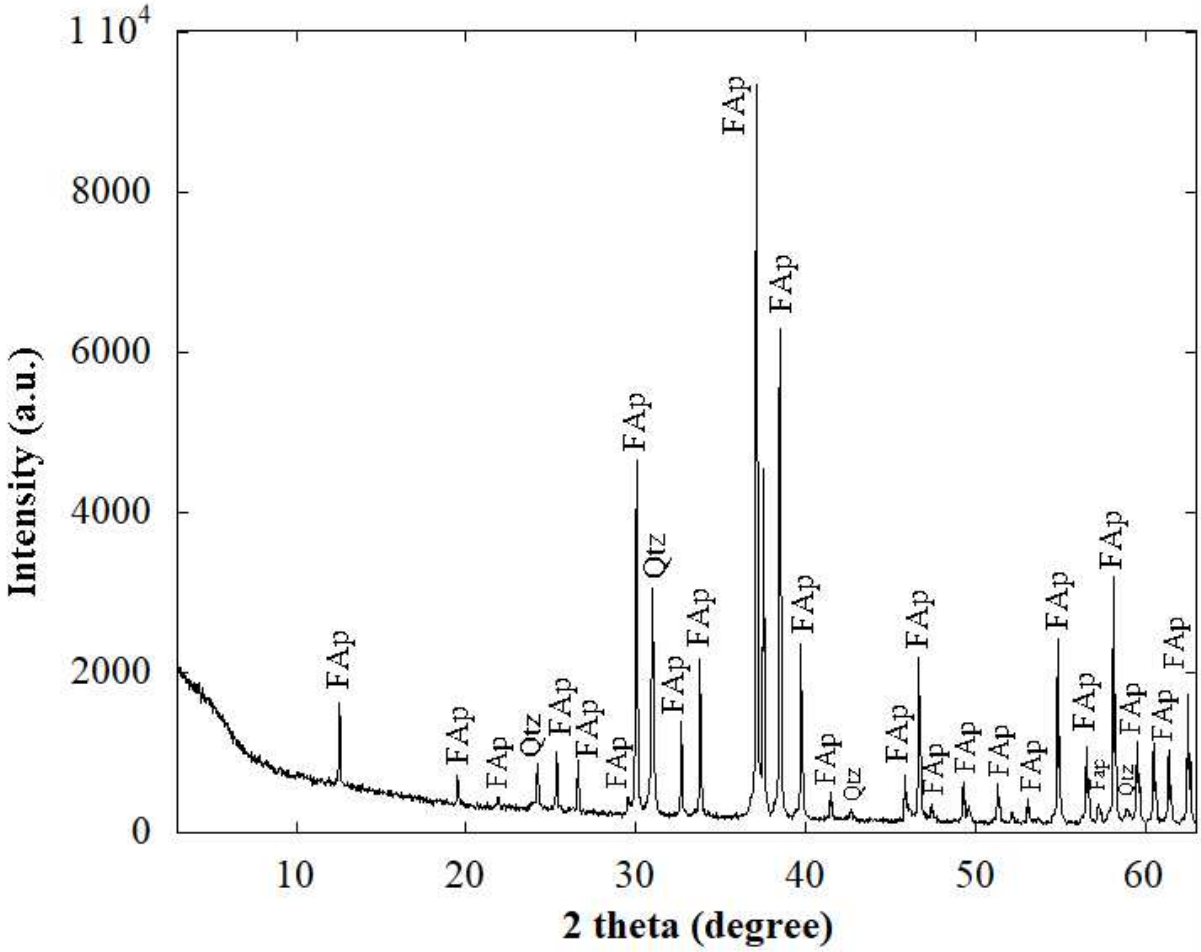

Fig. 1. XRD patterns of fluorapatite
(FAp: fluorapatite ; Qtz : Quartz).

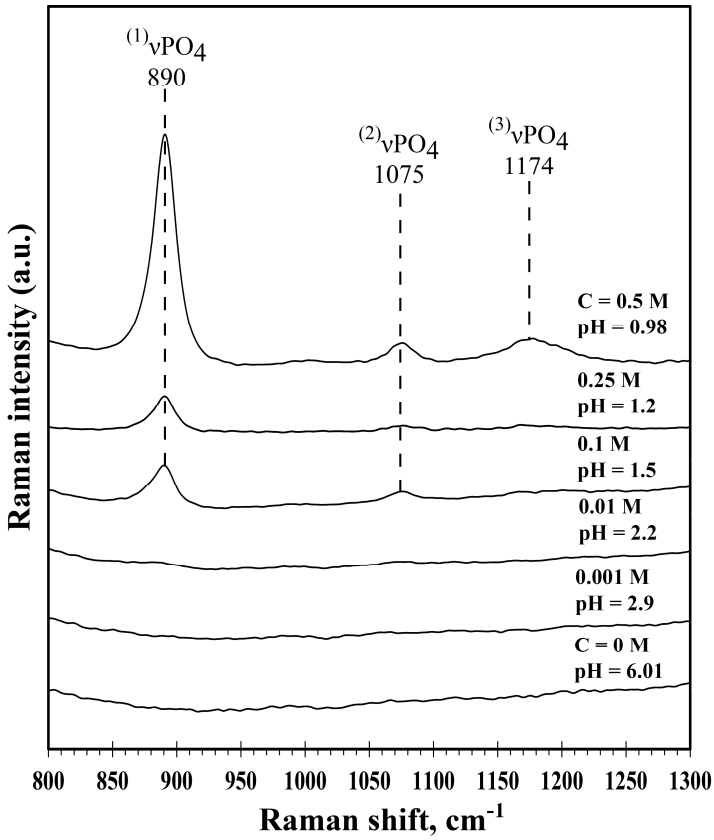

(1): P=O symmetric (H_3PO_4); (2) : P=OH symmetric (H_3PO_4); (3): P=O symmetric ($H_2PO_4^-$)

Fig. 2. Raman spectra of phosphoric acid in deionized water at different concentrations.

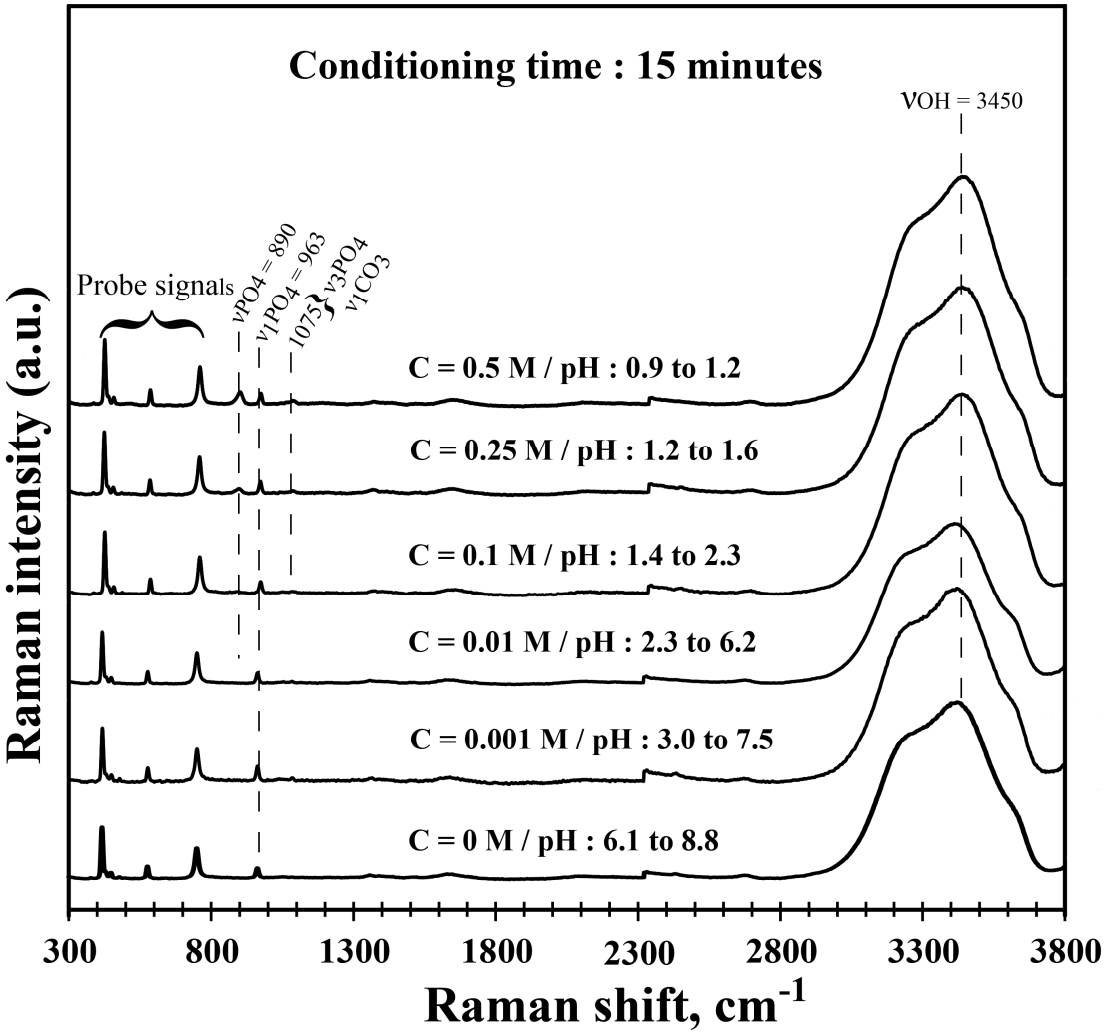

Fig. 3. Raman spectra of C-HFAp after 15 min of contact with solutions of phosphoric acid of different concentrations (300 to 3800 cm^{-1} region).

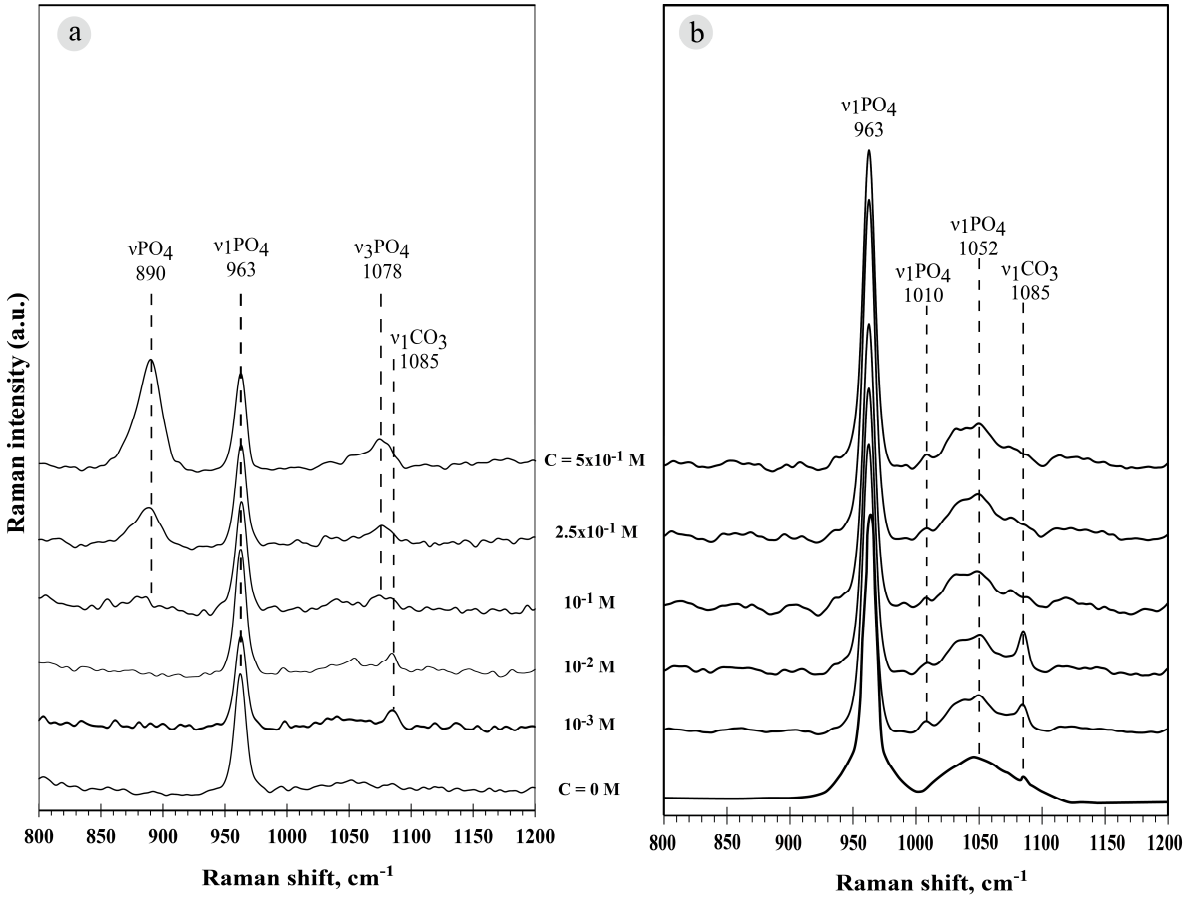

Fig. 4. Raman spectra of C-HFAp after 15 min of contact with solutions of phosphoric acid of different concentrations measured (a) *in-situ* and (b) after filtration and drying (800 – 1200 cm^{-1} region).

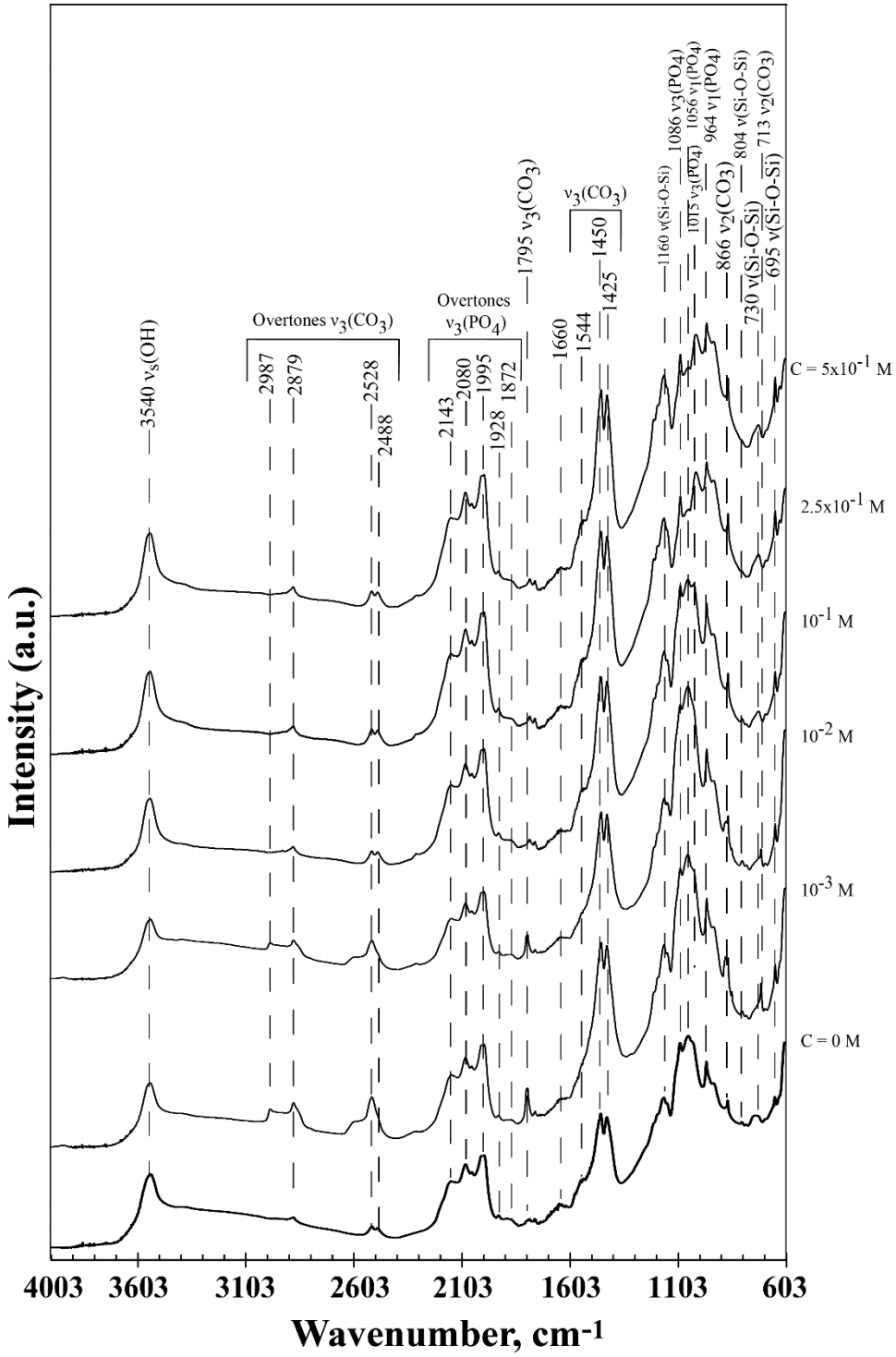

Fig. 5a. Infrared spectra (4003-603 cm^{-1} region) of C-HFAp which has been 15 min in contact with solutions of phosphoric acid of different concentrations.

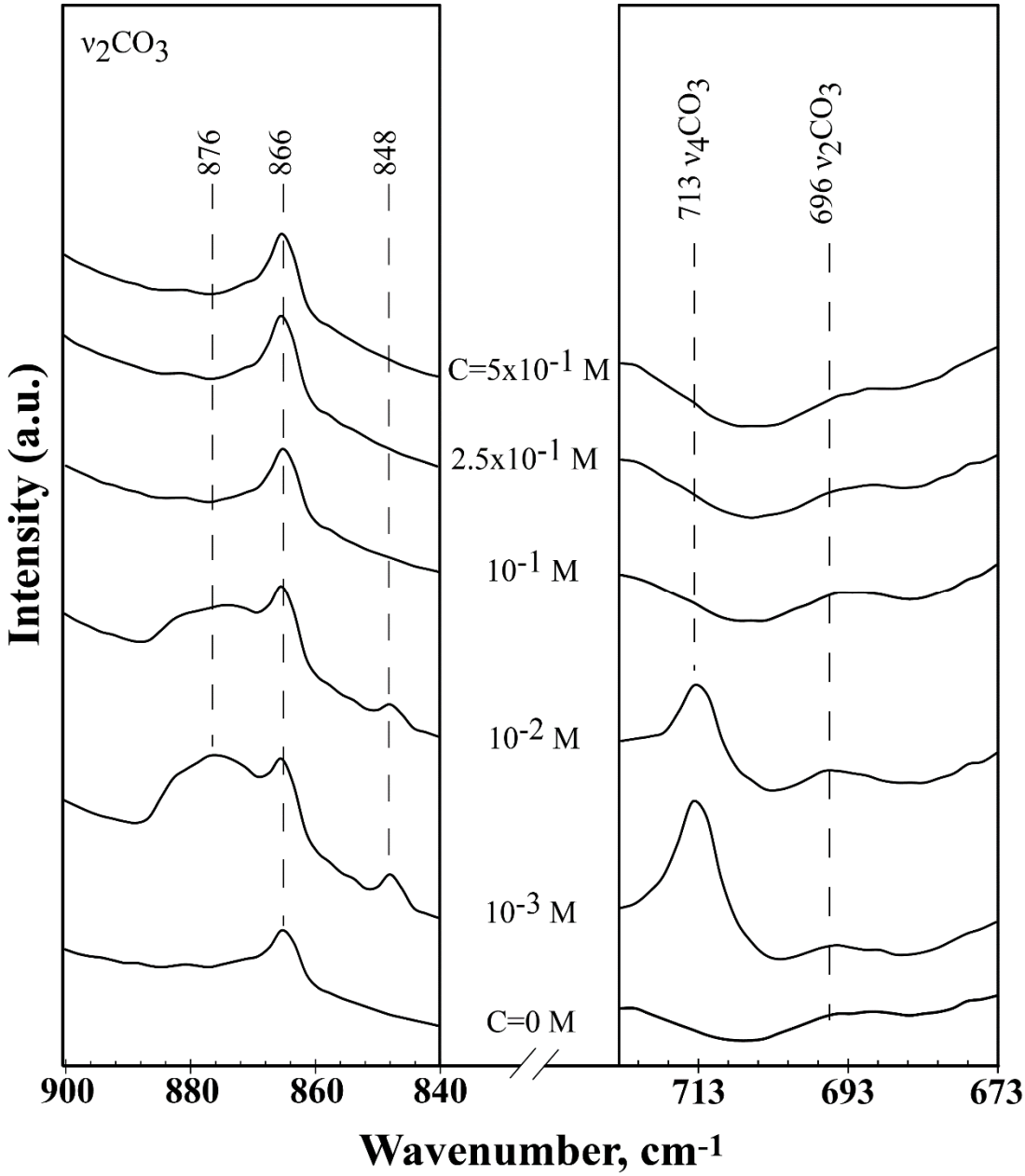

Fig. 5b. Infrared spectra (900-673 cm^{-1} region) of C-HFAp which has been 15 min in contact with solutions of phosphoric acid of different concentrations.

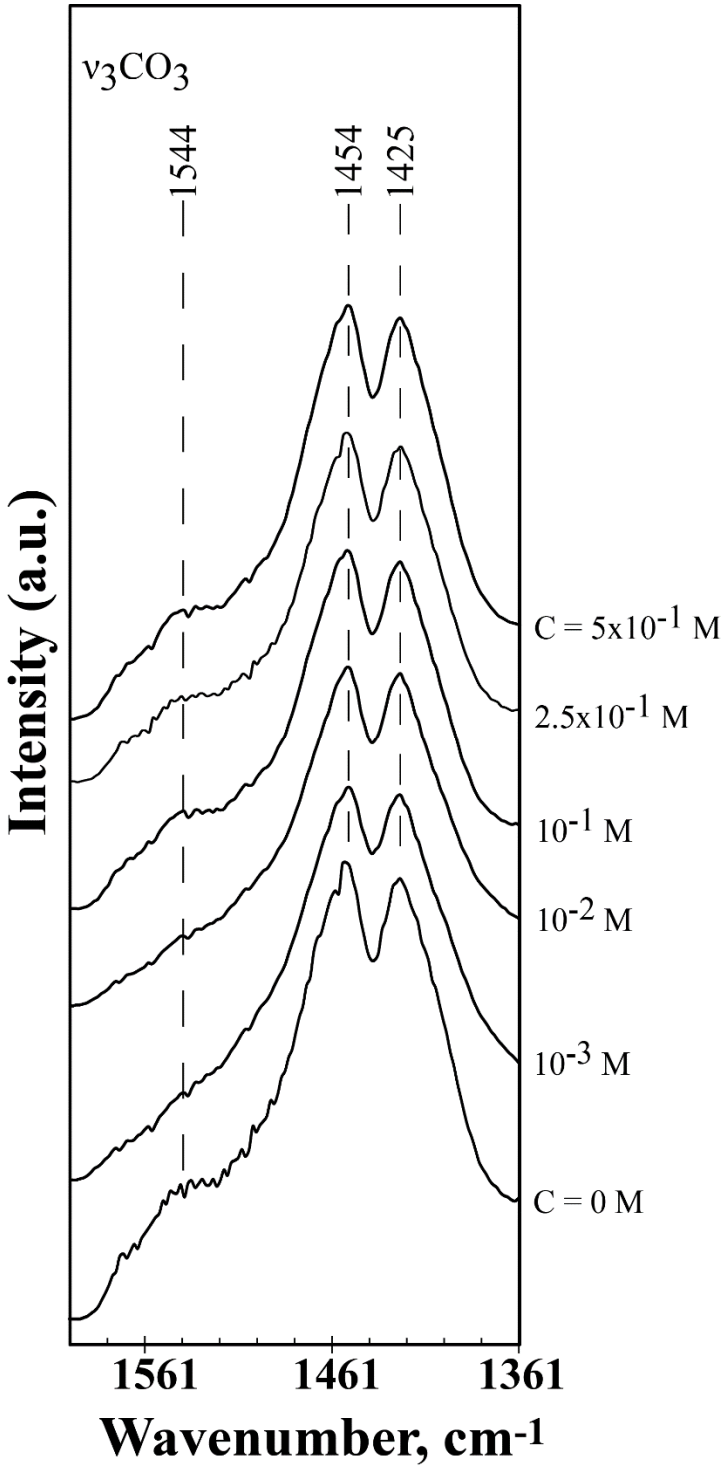

Fig. 5c. Infrared spectra (1602-1361 cm^{-1} region) of C-HFAp which has been 15 min in contact with solutions of phosphoric acid of different concentrations.

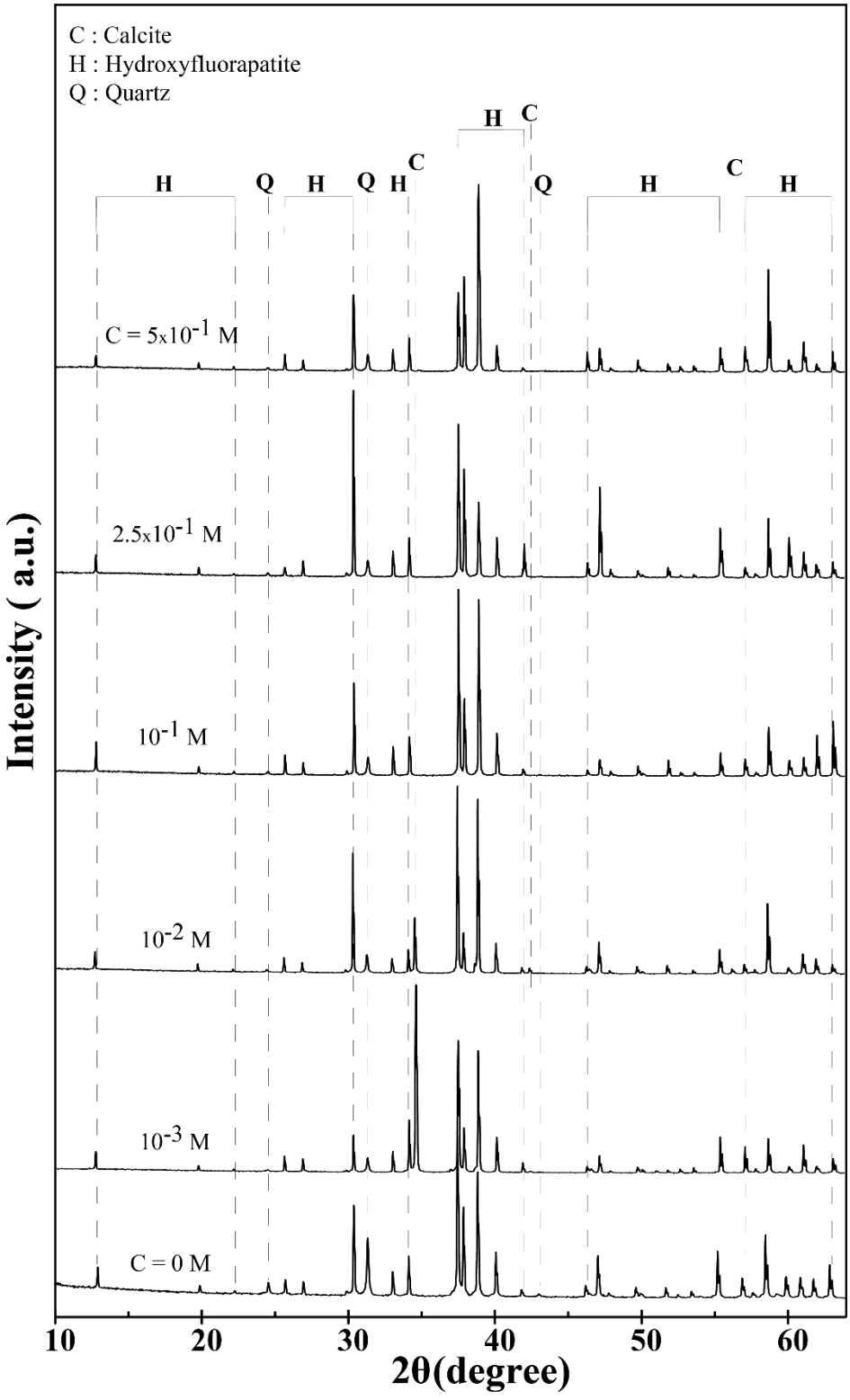

Fig. 6. XRD patterns of C-HFAp which has been 15 min in contact with solutions of phosphoric acid of different concentrations.

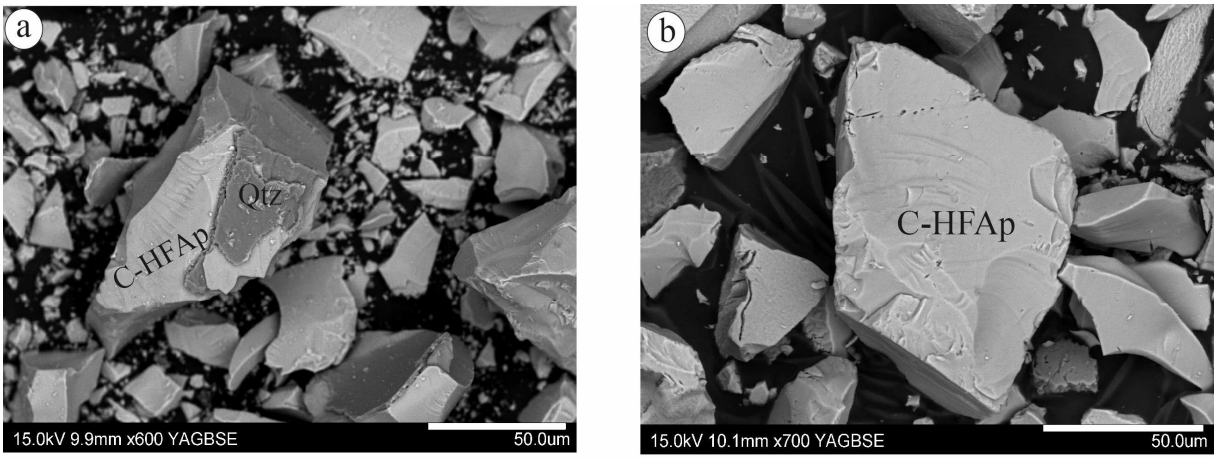

Fig. 7. SEM of C-HFAp after 15 min of contact with solutions of (a) 0 M, (b) 0.5 M phosphoric acid (C-HFAp: Hydroxyfluorapatite carbonated; Qtz: quartz).

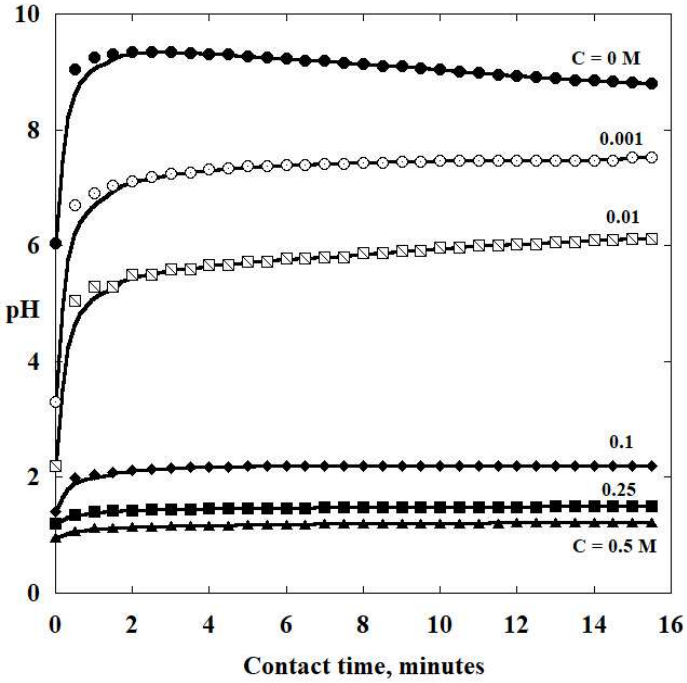

Fig. 8a. Change of C-HFAp pulp solution pH with time at different acid phosphoric concentrations.

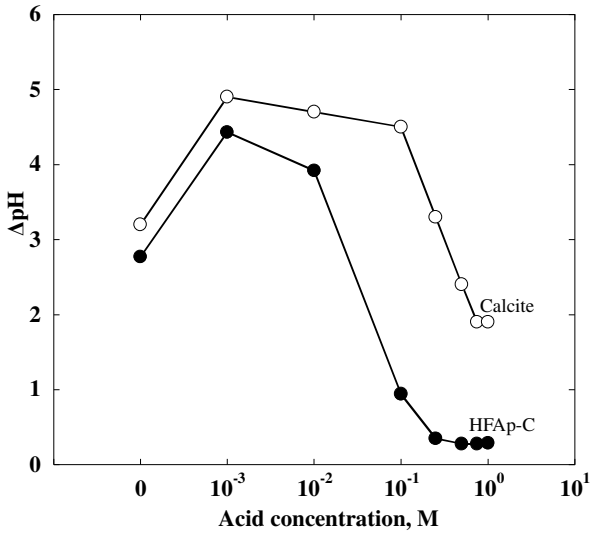

Fig. 8b. Change in pulp pH ($\Delta pH = pH_{t=15\ min} - pH_{t=0,\ without\ mineral}$) for C-HFAp and calcite as a function of phosphoric acid concentration.

Tables

Table 1. ICP-OES and ICP-MS analyses of fluorapatite

Oxides	CaO	P_2O_5	SiO_2	MgO	Al_2O_3	Fe_2O_3	Na_2O	K_2O	TiO_2	MnO	F	LOI
(%)	53.45	37.73	3.89	-	-	-	0.05	-	-	0.03	3.04	0.6

Elements	Ba	Ce	Cr	La	Nb	Rb	Sn	Sr	Th	Zn	Zr
(ppm)	6.86	2649	-	1214	2.89	0.57	-	549.2	1781	-	7.44

Table 2. Assignments of Raman bands from 1070 to 1088 cm^{-1} according to the type of minerals in the literature.

Raman wavenumber, cm^{-1}	Assignments according to literature	
	$\nu_1CO_3^{2-}$	$\nu_3PO_4^{3-}$
1070 in Carb-Ap	(Penel et al., 2003)* (Mandair and Morris, 2015)*	(Penel et al., 2003)* (Mandair and Morris, 2015)*
1071 in Carb-Hap	(Sakae, 2006)	
1073 in Carb-Hap		(Sakae, 2006)
1076 in Carb-Ap	(Mandair and Morris, 2015)*	(Mandair and Morris, 2015)*
1077 in Hap		(Penel et al., 2003)
1080 in HFAp 1080 in Hap		(Nathanael et al., 2013)
1081 in Fap		(Penel et al., 1997)
1084 in Brushite		(Kodati et al., 1991)
1085		(Juillard et al., 2010)
1086 in Calcite 1086 in Mg-phosphate	(Awonusi et al., 2007; Penel et al., 2000)	(Termine and Lundy, 1974)
1088 in Ca-phosphate		(Termine and Lundy, 1974)
1086-1088 in Carb-phosphate	(Termine and Lundy, 1974)	

(*) Authors suggests an overlap of ν_1CO_3 and ν_3PO_4 peaks. Carb-Ap: Carbonate-Apatite; Carb-HAp: carbonate hydroxyapatite; HAp: Hydroxyapatite; HFAp: Hydroxy-fluoroapatite; FAp: Fluorapatite; HFClAp: Hydroxy-fluoro-chloroapatite.

Table 3. Bands component analysis of the Raman and infrared spectra of C-HFAp.

Raman	IR	Assignments	References
	3540	OH stretching	(Arifuzzaman and Rohani, 2004)
3450		OH stretching	(de Ligny et al., 2013)
	2987 2879 2514	OH in carboxylic acids $\nu_3CO_3^{2-}$	(Lambert et al., 1987)
	2143 2080 1995 1872	$\nu_3PO_4^{3-}$	(Jouve, 1995)
	1795 1544 1454 1425	$\nu_3CO_3^{2-}$	(Farmer, 1975)
	1211	OH in plane bending	(Xu, 1996)
	1193 1160	ν(Si-O-Si)	(Arifuzzaman and Rohani, 2004)
	1140 1086	$\nu_3PO_4^{3-}$	(Frost et al., 2013; Sakae, 2006)
1140 1086		$\nu_3PO_4^{3-}$	(Juillard et al., 2010)
	1087	$\nu_1CO_3^{2-}$	(Potgieter-Vermaak et al., 2006)
1087 1086 1085		$\nu_1CO_3^{2-}$	(Klasa et al., 2013)
1078 1075		$\nu_3PO_4^{3-}$	(Brandão et al., 2009)
	1056	$\nu_3PO_4^{3-}$	(Gadaleta et al., 1996)
1052 1050		$\nu_3PO_4^{3-}$	(Awonusi et al., 2007)
	1020	$\nu_3PO_4^{3-}$	(Frost et al., 2013)
	964	$\nu_1PO_4^{3-}$	(Sakae, 2006)
963		$\nu_1PO_4^{3-}$	(Sakae, 2006)
	933	$\nu_1PO_4^{3-}$	(Grunenwald et al., 2014)
890		P=OH	(Brandão et al., 2009)
	876 866 848	$\nu_3CO_3^{2-}$	(Sakae, 2006)
	804 730	ν(Si-O-Si)	(Madejová and Komadel, 2001)
	713	$\nu_4CO_3^{2-}$	(Regnier et al., 1994)
	648	ν(Si-O-Si)	(Madejová and Komadel, 2001)

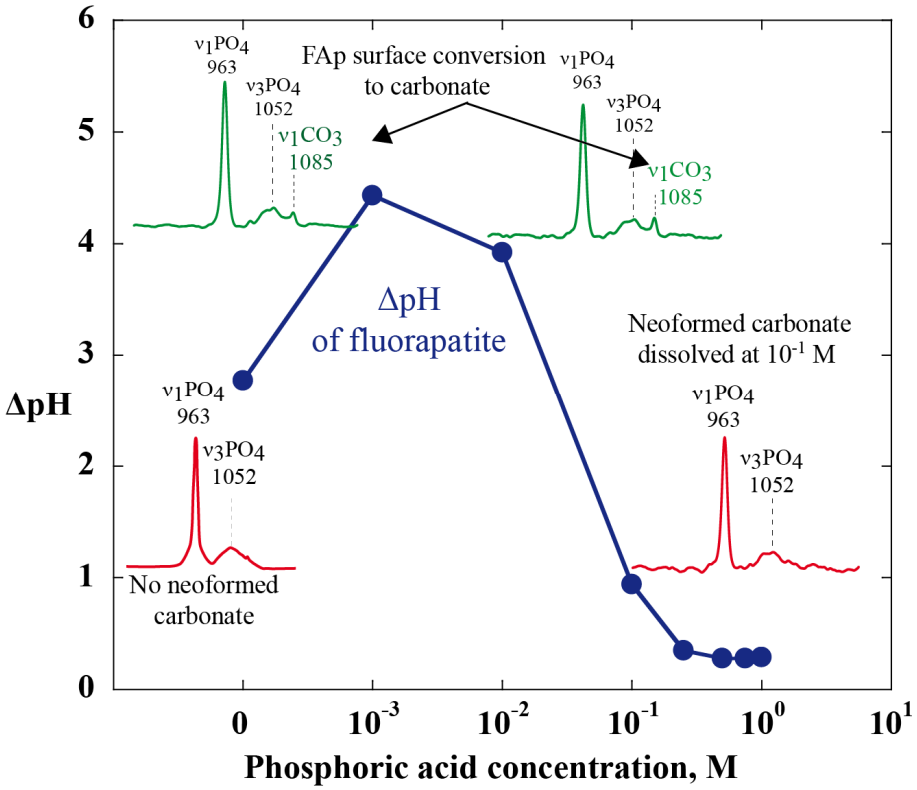
ΔpH
Phosphoric acid concentration, M
FAp surface conversion to carbonate
ν1PO4 963
ν3PO4 1052
ν1CO3 1085
ΔpH of fluorapatite
Neoformed carbonate dissolved at 10-1 M
No neoformed carbonate